Constitutive modeling of artificially cemented sand by considering fabric anisotropy

Zhiwei Gao, Jidong Zhao *

Department of Civil and Environmental Engineering, Hong Kong University of Science and Technology, Clearwater Bay, Kowloon, Hong Kong

ABSTRACT

Artificially cemented sand has been widely used in practical applications relevant to soil improvement and liquefaction mitigation. It has also been frequently used in laboratory tests to simulate the cementation and bonding formed in naturally structured sand. Known to be difficult to characterize, the behavior of artificially cemented sand is typically affected by its internal structure consisting of both bonding and fabric. In this study, a novel constitutive model is proposed to describe the effect of bonding and fabric anisotropy on the behavior of artificially cemented sand. We choose the triaxial tensile strength as a macroscopic representation of the inter-particle bonding, and a fabric tensor to characterize the fabric in sand. The yield function adopted in the model is an extension of a recently developed anisotropic failure criterion, with the frictional parameter therein being replaced by a proper hardening parameter. A de-bonding law is proposed by assuming the de-bonding process is driven by the development of plastic deformation. The soil fabric is kept constant in the study to account for inherent anisotropy. Relevant model parameters can be conveniently calibrated by conventional laboratory tests. The model is employed to predict the behavior of cemented Ottawa sand and multiple-sieving-pluviated Toyoura sand, and the predictions compare well with the experimental data.

© 2011 Elsevier Ltd. All rights reserved.

1. Introduction

Recent engineering practice witnesses an increasing interest in using artificial cementation to increase the stiffness and strength of problematic soils, for the purpose of controlling excessive displacement/settlement and/or liquefaction mitigation on relevant geo-structures [16,20,27,32,49,53]. Artificially cemented sand has also been widely used in laboratory testing to approximately reproduce the naturally formed structured sands [9,11,58]. The overall behavior of cemented sand thus depends crucially on the internal structure formed by cementation as well as particle/void arrangements in the sand. Proper characterization of the sand structure is key to effective modeling of cemented sand. It has been recognized that there are two controlling factors that contribute towards the important features of internal structure in sand, *bonding* and *fabric* [6,12,35].

The effect of bonding on artificially cemented sand has historically been a focus of numerous experimental studies. It has been found that bonding can help to stabilize the internal structure in sand and to increase its overall stiffness and peak strength [14,15,25,27,29,30]. Through artificial cementation, this feature of bonding has been widely exploited in practice to reduce the settlement in soft soils and to enhance the resistance of loose sand to liquefaction [20,41,53]. Meanwhile, it is also observed that the

post-peak behavior in cemented sand is much more brittle than clean sand and exhibits considerable stiffness degradation, due typically to the breakage of bonding [1,6,58]. Indeed, recent experiments have demonstrated that initiation of yielding of cemented granular materials is commonly accompanied by high rate of de-bonding [58]. The numerical simulations based on Discrete Element Method (DEM) have provided further support of the observations [58]. In addition, the bonding in sand may also have significant influence on the behavior of sand dilatancy as well. Triaxial compression tests [2,14,40,58] and torsional simple shear tests [32] show that sand cementation appears to be more dilative (or less contractive) than its untreated counterpart (clean sand) under otherwise identical loading conditions. Under undrained condition, greater dilation (or less contraction) implies that lower excess pore water pressure is caused by shear, and the sand is less vulnerable to liquefaction. From the perspective of volumetric change, this may help to explain why bonding can increase the liquefaction resistance of sand.

There have been numerous attempts in the past towards modeling the behavior of bonding in cemented sand. For example, based on the double-hardening concept, Hirai et al. [24] developed a two-yield-surface model with a modified Cam-clay plastic potential to describe bonding in cemented sand. Sun and Matsuoka [55] developed a model with the SMP criterion to model the bonding effect. In both models a cohesion parameter similar to the triaxial tensile strength [33] has been introduced to characterize the bonding. Sand structure in both models, however, has been assumed to

* Corresponding author. Tel.: +852 23588481.
E-mail addresses: gzwce@ust.hk (Z. Gao), jzhao@ust.hk (J. Zhao).

Nomenclature

A	anisotropic variable
b	intermediate principal stress ratio
d_{ij}	deviatoric fabric tensor
e	void ratio
e_{ij}, e_{ij}^e and e_{ij}^p	deviatoric strain, elastic and plastic strains respectively
F_{ij}	fabric tensor characterizing the initial fabric anisotropy
H	hardening parameter
I_1, I_2, I_3	invariants of the stress tensor
$\bar{I}_1$, $\bar{I}_2$, $\bar{I}_3$	invariants of the transformed stress tensor
p and $\bar{p}$	mean stress and transformed mean stress
p_r	reference pressure
q and $\bar{q}$	deviatoric stress and transformed deviatoric stress
s_{ij} and $\bar{s}_{ij}$	deviatoric stress tensor and transformed deviatoric stress tensor
α	parameter for the yield function
δ_{ij}	Kronecker delta
Δ	parameter characterizing the degree of inherent fabric anisotropy
ε_1, ε_2, ε_3	major, intermediate and minor principal strain respectively
ε_q, ε_q^e and ε_q^p	total, elastic and plastic deviatoric strain in triaxial space
ε_v, ε_v^e and ε_v^p	total, elastic and plastic volumetric strain
θ	angle between the current stress state and the vertical stress axes in the deviatoric plane (see Fig. 1)
ξ	angle between the major principal stress and direction of deposition
σ_0	triaxial tensile strength
σ_1, σ_2, σ_3	major, intermediate and minor principal stress respectively
$\bar{\sigma}_1$, $\bar{\sigma}_2$, $\bar{\sigma}_3$	transformed major, intermediate and minor principal stress respectively
σ_c	confining pressure in triaxial compression tests
σ_{ij} and $\bar{\sigma}_{ij}$	stress tensor and transformed stress tensor
σ_x, σ_y, σ_z	stresses in the x, y and z directions respectively

remain intact during the deformation of the soil, which prevents them from adequately describing the post-peak degradation of shear modulus that is believed to be caused mainly by de-bonding [1,58]. To tackle this issue, various de-bonding laws have been proposed thereafter [34,45]. A common way in these studies is to assume that both the size and location of the yield surface are dependent on the degree of bonding and the evolution of the yield surface naturally involves the effect of de-bonding. A variety of other approaches and concepts have also been developed to describe de-bonding in cemented sand, e.g., the concept of disturbed state by Desai and Toth [15], the damage-based approaches [28] followed by Chazallon and Hicher [8], Yu et al. [60] and Namikawa and Mihira [43], the multi-phase models [1,56] as well as the multi-scale approach [23].

Apart from bonding, fabric is another important factor influencing the sand response. Fabric is formed in soil during its deposition and compaction processes and may collectively reflect the grain gradation, density, interlocking and anisotropy (e.g., particle shape and orientation, void distribution, contact normal distribution etc.) [7,37,38,46,59]. In particular, fabric anisotropy has long been regarded an important factor attributable to many complicated macroscopic behavior in sand [39,47]. Under the influence of either compaction or gravitational force which is typically one-dimensional, sand particles deposits and forms typical fabric structure with cross-anisotropy (or transverse-isotropy) which is characterized by one direction with distinctive anisotropy perpendicular to a bedding or lamination plane wherein it is largely isotropic. This perpendicular direction, normally coincident with the direction of deposition, is referred to as the axis of anisotropy. The effect of fabric on sand behavior (stiffness, strength and dilatancy) has long been recognized in clean sand [42,57,59] and natural clay [44]. Less attention, however, has been paid to the characterization and modeling of fabric anisotropy in cemented sand. Indeed, the impact of fabric anisotropy on the overall behavior of cemented sand is equally important as in clean sand. This is proved by a recent series of tests carried out by Saebimoghaddam [52] who found from triaxial compression tests (the major principal stress is applied in the direction of deposition) and triaxial extension tests (the major principal stress direction aligns in the deposition plane) on a cemented paste backfill that the material shows less contractive and stiffer response in triaxial compression. The observed discrepancy under the two loading conditions is evidently caused

by fabric anisotropy. There have been numerous studies in the literature focusing on the effect of fabric anisotropy in sand, such as the models based on yield surface rotation [54], bounding surface models [13,37,38] and many others. We shall not attempt herein a lengthy literature survey on this topic. A relatively detailed review on fabric anisotropy can be found in Gao et al. [21].

Apparently, both bonding and fabric anisotropy contribute to important characteristics of the strength and deformation of cemented sand. Failure to fully account for either of them may result in serious consequences in the design and construction of geostructures relevant to naturally or artificially cemented sand, such as foundation and engineered slopes [1,2,12,27]. Frequently, the two aspects of soil structure cannot completely be separated. They combine to affect the behavior of sand as a whole. It is hence desirable to have a constitutive model to consider them comprehensively in modeling the behavior of cemented sand. Unfortunately, most existing constitutive models are concerned either with the effect of bonding only, or are devoted to the anisotropic effect alone (e.g., for clean sand). One exception might be the bounding surface model recently proposed by Belokas and Kavvadas [4] which was developed to simulate the general structural effect on both sand and clay. Its performance on simulating the behavior of cemented sand, however, has not been verified. We also notice that there are a great number of investigations on modeling the effect of structure in natural clay [3,18,19,31,61]. While we are concerned with cemented sand here only, a comprehensive review and comparison of these studies are beyond the scope of this paper.

In view of the unsatisfactory status quo on the modeling of cemented sand, a simple and novel elasto-plastic model will be proposed in this paper. This has indeed been motivated by a previous work by the authors on anisotropic failure criterion for geomaterials [22]. This failure criterion has been proved to be versatile and general and have been used to characterize the strength anisotropy for a wide range of materials, including sands, clays and rocks. We have found that through replacing the constant frictional parameter in the criterion by a properly chosen hardening parameter, this criterion can be easily adapted to a good yield function to describe the effects of both bonding and fabric anisotropy, which is hence suitable for the modeling of cemented sand. The bonding effect can be easily described by the triaxial tensile strength in this criterion together with a newly proposed evolution law for debonding. Meanwhile, the anisotropic effect may be still conveniently

characterized by an anisotropic variable defined by a joint invariant of the stress tensor σ_{ij} and the fabric tensor F_{ij}. With some further additions of incremental elastic relation and hardening laws, a new yet simple constitutive model for artificially cemented sand is developed. We further use test results on cemented Ottawa sand [58] and Multiple-sieving-pluviated (MSP) Toyoura sand [42] to verify the predictive capability of the model. The comparisons appear to be encouragingly good. Towards the end of the paper, we also discuss some limitations and potential improvements of the model.

2. Characterization of bonding and fabric in cemented sand

Soil structure comprises of fabric and inter-particle force system that reflect all facets of the soil composition, history, present state, and environment, and therefore is complex in nature. Interparticle bonding in artificially cemented sand is related to the properties of cementing agent and cement content [2,5,9,10,58]. It is found that stronger cementing agent with higher unit weight may lead to stronger bonding strength [58]. Quantitative measurement of the true interparticle bonding at the particle level in soils proves to be difficult. However, some macroscopic observable quantities can be used as alternatives to characterize the bonding in soils. For instance, experimental observations show that for the strong bonding case [12,51], cemented soil has a gross yield stress greater than that of its un-cemented/reconstituted counterpart in one-dimensional or isotropic compression tests. The difference between the gross yield stresses can hence be used as an index to quantify the bonding. For soils with weak bonding [12], however, the difference is normally insignificant. As such, this difference is not always a suitable quantity to measure bonding. Nevertheless, for both the weak and strong bonding cases, experimental studies have observed an obvious peak strength state when a sample is subjected to triaxial compression at low confining pressure, which is due primarily to the contribution of interparticle bonding [12,40,58]. We hereby employ the triaxial tensile strength of a material, σ_0 [33], as a macroscopic counterpart to the particle-scale bonding, to account for its contribution to the peak strength of a soil. Its value can be determined indirectly, e.g., via back calculation from experimental data on the peak strength of a soil [22,33].

To describe the behavior of fabric in naturally/artificially cemented sand, we shall employ a symmetric second-order fabric tensor originally proposed by Oda and Nakayama [47]. In view of the fact that most soils are cross-anisotropic, we assume that the principal axes of soil fabric is aligned with a reference coordinate system (x_1, x_2, x_3), wherein the $x_2 - x_3$ plane defines the isotropic plane of the fabric, and the x_1 axis points to the direction of anisotropy. Consequently, the following simplified form of fabric tensor may be adopted for the description of cross-anisotropy in the soil

$$F_{ij} = \begin{bmatrix} F_1 & 0 & 0 \\ 0 & F_2 & 0 \\ 0 & 0 & F_3 \end{bmatrix} = \frac{1}{3+\Delta} \begin{bmatrix} 1-\Delta & 0 & 0 \\ 0 & 1+\Delta & 0 \\ 0 & 0 & 1+\Delta \end{bmatrix} \quad (1)$$

where Δ is a scalar that characterizes the magnitude of the cross-anisotropy [47]. Its value ranges from zero when the material is absolutely isotropic, to unity when the degree of anisotropy is the maximum. If the observation coordinate or material has been rotated, the fabric tensor expressed in Eq. (1) may be subjected to orthogonal transformation.

3. Model description

The model will be developed within the framework of classic plasticity. Essential components of an elasto-plastic model as

required by a standard plasticity theory, such as the yield function, dilatancy, flow rule as well as the elastic relation, will be specified.

3.1. Yield function

It has long been recognized that the yielding and strength of sand is dependent not only on the current stress state and the loading history, but also on the internal structure as well as the loading direction relative to the internal structure. Meanwhile, a yield function should satisfy the requirement of objectivity and needs to be independent of the choice of coordinate system. In this connection, it is assumed the yielding behavior of a sand with structure can be expressed as a general isotropic function of the stress tensor σ_{ij}, the fabric tensor F_{ij}, the triaxial tensile strength σ_0 and some other internal variables ζ_n as follows,

$$f = f(\sigma_{ij}, F_{ij}, \sigma_0, \zeta_n) = 0 \quad (2)$$

Specific forms of the stress tensor and fabric tensor, and/or the internal variables need to be expressed in forms of invariants to guarantee the objectivity condition. In this paper, we propose the following yield function to describe the yielding of sand which considers both bonding and fabric

$$f = \alpha\sqrt{\bar{I}_1^2 - 3\bar{I}_2} + \frac{2(1-\alpha)\bar{I}_1}{3\sqrt{(\bar{I}_1\bar{I}_2 - \bar{I}_3)/(\bar{I}_1\bar{I}_2 - 9\bar{I}_3)} - 1} - \frac{1}{3}Hg(A)\bar{I}_1$$
$$= 0 \quad (3)$$

The above yield function is indeed modified from a general anisotropic failure criterion recently proposed by the authors [22] wherein we simply replace the originally constant frictional coefficient M_f with a hardening parameter H. In Eq. (3), α is a model parameter. $\bar{I}_1$ $(= \bar{\sigma}_1 + \bar{\sigma}_2 + \bar{\sigma}_3)$, $\bar{I}_2$ $(= \bar{\sigma}_1\bar{\sigma}_2 + \bar{\sigma}_2\bar{\sigma}_3 + \bar{\sigma}_1\bar{\sigma}_3)$ and $\bar{I}_3$ $(= \bar{\sigma}_1\bar{\sigma}_2\bar{\sigma}_3)$ are invariants of a transformed stress tensor $\bar{\sigma}_{ij}$ defined below [22,33]

$$\bar{\sigma}_{ij} = \sigma_{ij} + \sigma_0\delta_{ij} \quad (4)$$

where δ_{ij} is the Kronecker delta with $\delta_{ij} = 1$ when $i = j$ and $\delta_{ij} = 0$ when $i \neq j$. Note that the curvature of the yield curve in the meridian plane is neglected by setting the parameter n used in Gao et al. [22] to be unity. Key to the yield function in Eq. (3) is the anisotropic function defined as

$$g(A) = \exp\{d[(A+1)^2 + \beta(A+1)]\} \quad (5)$$

where d and β are two constants and A is an anisotropic variable describing the relative orientation of the loading direction to the fabric which is defined by

$$A = \frac{s_{ij}d_{ij}}{\sqrt{s_{mn}s_{mn}}\sqrt{d_{pq}d_{pq}}} \quad (6)$$

where s_{ij} $(= \sigma_{ij} - \sigma_{kk}\delta_{ij}/3)$ and d_{ij} $(= F_{ij} - F_{kk}\delta_{ij}/3)$ denote the deviatoric stress tensor and deviatoric fabric tensor, respectively. Note that due to normalization, the value of Δ does not affect the value of A. For more discussion on the variation of A under typical loading conditions, please refer to Gao et al. [22]. In essence, d plays a role of measuring the degree of strength anisotropy for a material. When $d = 0$, we see that $g(A) \equiv 1$, irrespective of the loading direction. In this case, the yield function defined in Eq. (3) is isotropic in the stress space. Notably, the anisotropic yield function is identical to the isotropic one in conventional triaxial compression state wherein the major principal stress direction is perpendicular to the deposition plane, since $A \equiv 1$ at this state. With the involvement of fabric tensor, however, the anisotropic yield locus usually cannot be directly visualized in the conventional deviatoric plane as conventional (isotropic) yield functions do. Nevertheless, under some special conditions this is still possible. For example, in true triaxial
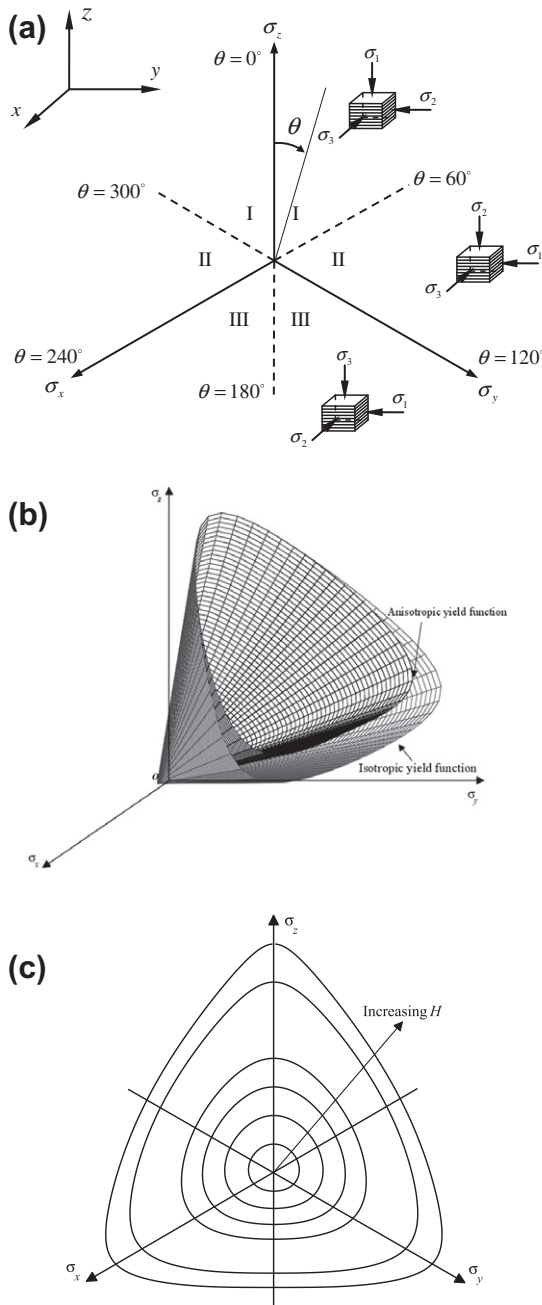
Fig. 1. (a) Definition of the angle θ and partition of the deviatoric plane under the true triaxial test condition (after [46]); (b) the yield surface in the three-dimensional space and (c) the yield loci in the deviatoric plane.

tests if both the stress direction and the fabric orientation are set to align in the same fixed coordinate, such as the cases shown in Fig. 1a, the yield surface can be plotted as shown in Fig. 1b (the yield surfaces do not cross the origin of the coordinate system due to the existence of bonding) and Fig. 1c (yield loci in the deviatoric plane with different values of hardening parameter). The isotropic failure surface is shown in the deviatoric plane in comparison with the anisotropic one. Note that in Fig. 1a we denote the angle between the current stress state with the vertical stress axes in the deviatoric plane by θ, and the deviatoric plane is partitioned into three zones as shown in Fig. 1a. The same convention will be followed in the subsequent sections.

3.2. Hardening law

The following evolution law for H is proposed:

$$dH = \langle dL \rangle r_H = \langle dL \rangle \frac{G c_h \zeta}{H p_r}(M_f - H) \tag{7}$$

where r_H denotes the evolution direction of H and is always greater than or equal to zero; dL is a loading index and $\langle x \rangle$ denotes the Macauley bracket with $\langle x \rangle = 0$ when $x \leqslant 0$ and $\langle x \rangle = x$ when $x > 0$; c_h is a positive constant. Following Li and Dafalias [37] and Dafalias et al. [13], we introduce the following ζ as a scaling factor to account for the effect of fabric anisotropy on the soil stiffness

$$\zeta = \exp[-k(A + 1)] \tag{8}$$

where k is a positive model parameter. Evidently, ζ in form of Eq. (8) is a decreasing function of A. This is supported by experimental observations that, under otherwise identical conditions, the response of a soil becomes softer as the major principal stress direction deviates away from the direction of deposition (A decreases with this change) [42,59]. Note that in case of conventional triaxial compression with the axis of deposition co-axial with the axial compression direction, $A = -1$, such that $\zeta \equiv 1$. The special feature of this shear mode makes it suitable to be used as a reference for model calibration, which will be discussed in a later section.

Experimental observations [1,58] show that the bonding of soils is gradually weakened due to the development of plastic deformation, which leads to significant degradation in shear modulus during the post peak stage. In the present model, a simple linear relation between the rate of de-bonding and the plastic deviatoric strain increment is assumed,

$$d\sigma_0 = \langle dL \rangle r_0 \tag{9}$$

where

$$r_0 = \begin{cases} -m(H/M_f)^{2000}\sigma_0 & \text{for } \sigma_0 > 0 \\ 0 & \text{for } \sigma_0 \leqslant 0 \end{cases} \tag{10}$$

where σ_0 denotes the current triaxial tensile strength of the material and m is a non-negative model parameter. The above evolution law ensures that r_0 is always less than or equal to zero and the process of de-bonding proceeds steadily with plastic straining until σ_0 reaches zero. It is assumed that elastic deformation does not cause de-bonding in this evolution law. Since the initial value of the triaxial tensile strength σ_{0i} is determined based on the peak strength state of cemented sand (see the case for cemented Ottawa sand shown in Fig. 2), the term $(H/M_f)^{2000}$ is used to force the de-bonding rate to become very small before the peak strength state.

3.3. Dilatancy and flow rule

Dilatancy relation is the cornerstone of a constitutive model for sand. To incorporate the effect of bonding and fabric anisotropy into the dilatancy of sand, we propose the following dilatancy relation based on the work by Li and Dafalias [37],

$$D = \frac{d\varepsilon_v^p}{\sqrt{2/3 de_{ij}^p de_{ij}^p}} = \frac{d_1}{\exp(\int \langle dL \rangle)}(M_p d_C d_F - H) \tag{11}$$

where $d\varepsilon_v^p$ is the plastic volumetric strain increment; de_{ij}^p ($= d\varepsilon_{ij}^p - d\varepsilon_v^p \delta_{ij}/3$) is the plastic deviatoric strain increment; d_1 is a positive model parameter; M_p is the phase transformation stress ratio measured in conventional triaxial compression tests on remolded samples. The role of the denominator in Eq. (11) is to control the volume change, especially when the strain level is high. As the sample is sheared to the critical state, the increment of plastic deviatoric strain will not be limited. As such the denominator term
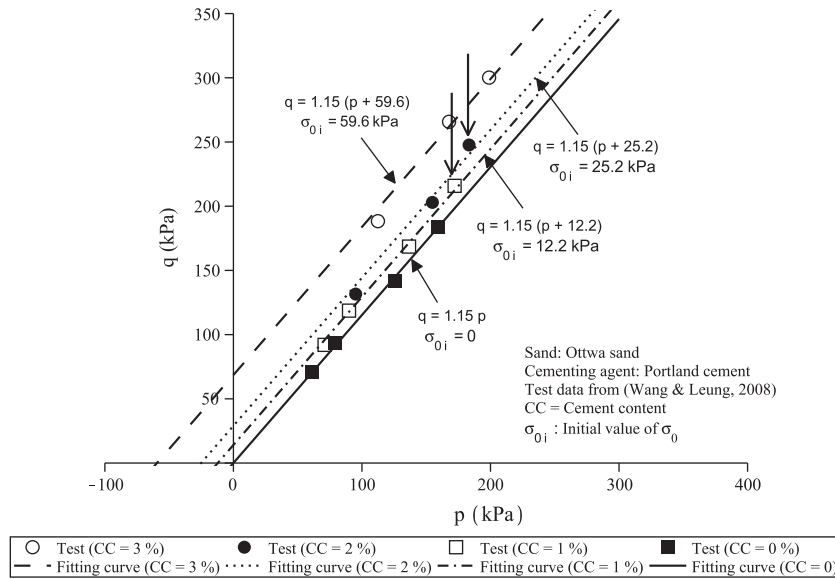
Fig. 2. Peak strength of cemented Ottawa sand [58] and the fitting curves with the same slope measured from the results on un-cemented samples.

will reach infinity with unlimited flow, which makes the value of D approach 0. The two scaling factors d_C and d_F are used to characterize the bonding and anisotropic effects, respectively,

$$d_C = \exp\left(-c_0\sqrt{\sigma_0/p_r}\right) \tag{12}$$

$$d_F = \exp[k(A+1)] = \frac{1}{\zeta} \tag{13}$$

where c_0 is a positive model constant and k is the same one as in the expression of ζ in Eq. (8). By this dilatancy relation in Eq. (11), as the value of σ_0 increases, d_C decreases such that D becomes smaller. The soil response is hence less contractive and the liquefaction resistance potentially increases [14,20,53]. d_F is indeed a reciprocal form of ζ defined in Eq. (8) which describes the dilatancy anisotropy of sand (see also [13,37]). Under otherwise identical conditions, d_F increases with A (the major principal stress direction deviates more away from the direction of deposition), which in turn leads to bigger value of D and more contractive soil response [42,59].

Meanwhile, based on the yield function in Eq. (3), we propose the following associated flow rule

$$de_{ij}^p = \langle dL \rangle n_{ij} \tag{14}$$

where n_{ij} is a unit tensor defined by

$$n_{ij} = \frac{1}{B}\left(\frac{\partial f}{\partial \sigma_{ij}} - \frac{1}{3}\frac{\partial f}{\partial \sigma_{mn}}\delta_{mn}\delta_{ij}\right) \tag{15}$$

where B is the norm of the quantity in the parentheses in Eq. (15). Note that a similar flow rule has also been used by Pietruszczak [48].

3.4. Elastic moduli

The elastic response of sand typically exhibits a dependence on pressure and density, which leads to a nonlinear elastic behavior. Richart et al. [50] have proposed an empirical relation to describe this nonlinear behavior for the elastic shear modulus, G, of sand which has been proved suitable for a variety of sands [13,37–39]. Based on the expression proposed by Richart et al. [50], with further postulate that the de-bonding process also affects the elastic behavior of sand, the following modified nonlinear form of G is assumed in this paper

$$G = G_0 \exp\left(\sqrt{\frac{\sigma_0}{p_r}}\right)\frac{(2.97-e)^2}{1+e}p_r\sqrt{\frac{p}{p_r}} \tag{16}$$

where G_0 denotes a material constant; p_r is a reference pressure which is normally chosen to be the atmospheric pressure

Table 1
Model parameters for cemented Ottawa sand [58], multiple-sieving pluviated (MSP) Toyoura sand [42] and model illustration.

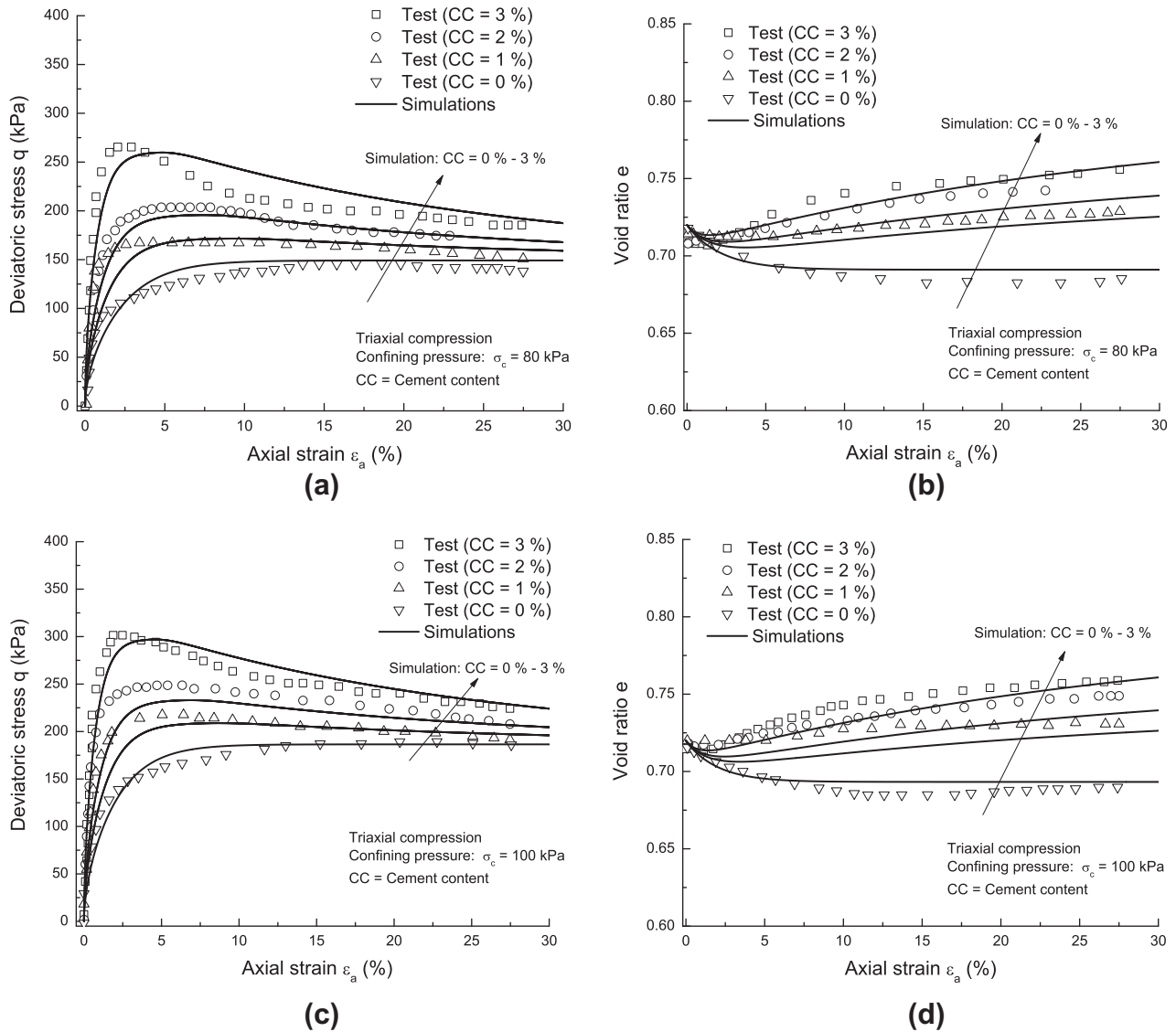| Parameter		Cemented Ottawa sand	MSP Toyoura sand	Model illustration
Failure	M_f	1.15	1.55	1.15
	α	0	0.51	0
	d	0	−0.16	−0.05
	β	0	−0.42	0
Elastic moduli	G_0	123	125	123
	v	0.01	0.2	0.01
Hardening law	c_h	0.1	0.35	0.1
	k	0	0.25	0.04
	m	3.5	0	3.5
Dilatancy	d_1	1.1	1.0	1.1
	M_p	1.15	1.0	1.15
	c_0	0.15	0	0.15

Fig. 3. Comparison between the model predictions and tested results on cemented Ottawa sand in drained triaxial compression with the confining pressure of 80 kPa (a and b) and 100 kPa (c and d).

(101 kPa); $\bar{p}$ is the transformed mean stress; $\exp(\sqrt{\sigma_0/p_r})$ is a new term introduced to the original form of Richart et al. [50] to account for the influence of bonding to the elastic response of sand [17,25]. The elastic bulk modulus, K, is assumed to depend on G and the Poisson's ratio v according to

$$K = G\frac{2(1+v)}{3(1-2v)} \tag{17}$$

where v is assumed to be a constant here.

4. Model calibration and verification

4.1. Calibration of model parameters

To begin with, it is instructive to discuss the calibration of model parameters. The determination of relevant parameters involved in the original anisotropic failure criterion has been discussed in detail in Gao et al. [22] which will not be repeated here. Nevertheless, we emphasize that the initial value of the triaxial tensile strength σ_{0i} must be specified in order for the de-bonding process to be properly considered. For each case of cement content, it is ob-

tained from the intersection of the peak strength fitting curve with the hydrostatic axis (Fig. 2). The other parameters to be calibrated can be roughly classified into three groups, those parameters relevant to the elastic moduli, the parameters for the hardening law and the parameters for the dilatancy relation. All of them can be readily calibrated from the conventional triaxial compression and extension tests, by following the procedure outlined below.

(a) G_0: Based on the expression for the elastic shear modulus, the parameter G_0 can be calibrated using the small strain stiffness tests on un-bonded (clean cohesionless) sand. Alternatively, it can be determined by fitting the $q - \varepsilon_q$ curve at the initial elastic range under either drained or undrained conditions, where $\varepsilon_q \left(= \sqrt{2/3 de_{ij}^p de_{ij}^p}\right)$ is the magnitude of the deviatoric strain.

(b) M_p: The phase transformation stress ratio M_p can be readily obtained from the conventional triaxial compression tests on un-bonded clean soil samples.

(c) d_1: Neglecting the small elastic deformation, one has the following relation under the drained triaxial compression condition for un-bonded sand samples,
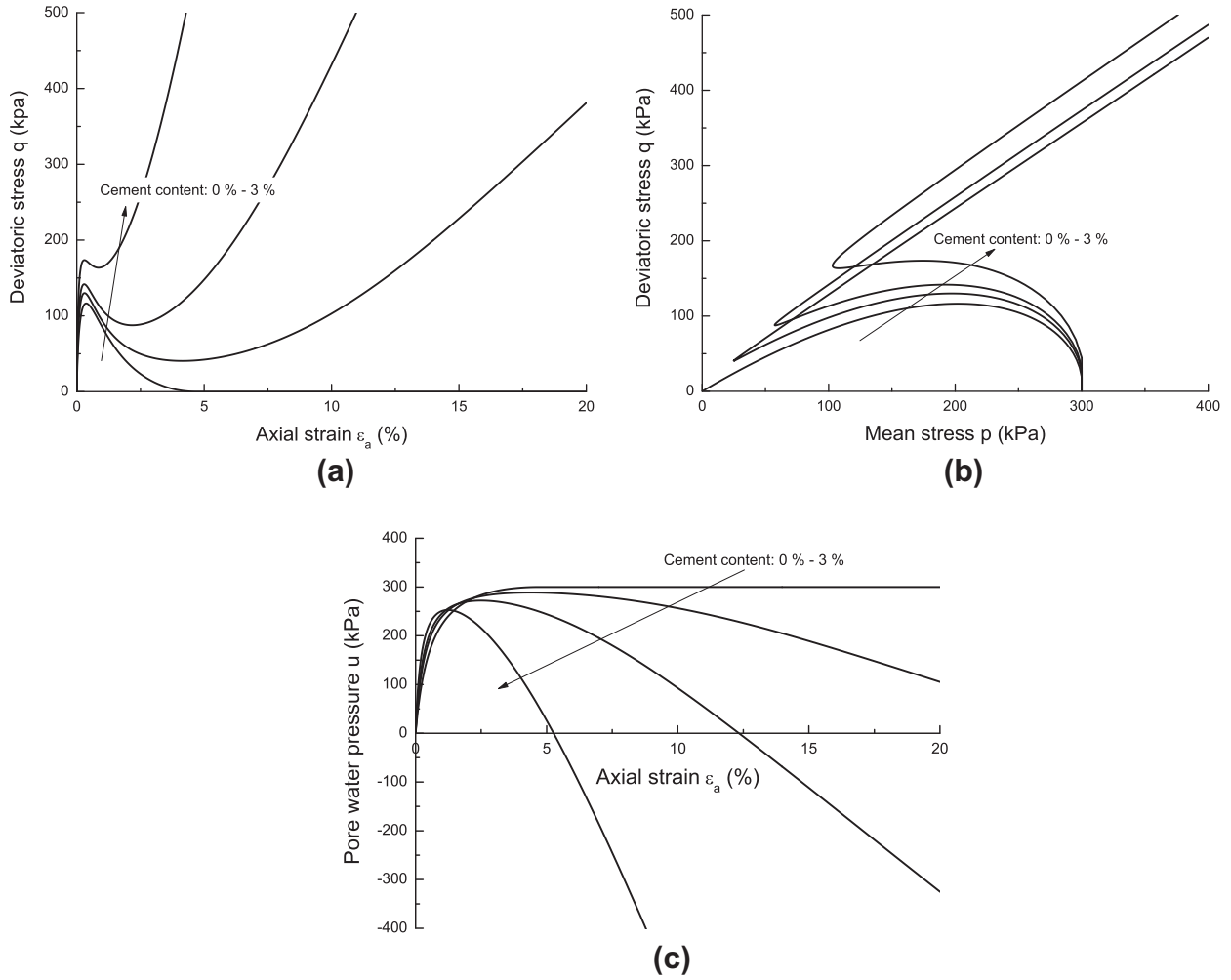
Fig. 4. Model simulations for the response of cemented Ottawa sand in undrained triaxial compression: (a) $\varepsilon_a - q$ relation; (b) $p - q$ relation and (c) $\varepsilon_a - u$ relation.

$$\frac{d\varepsilon_v^p}{d\varepsilon_q^p} \approx \frac{d\varepsilon_v}{d\varepsilon_q} = \frac{d_1}{\exp\left(\sqrt{3/2}\varepsilon_q\right)}\left[M_p \exp\left(-c_0\sqrt{\frac{\sigma_0}{p_r}}+k(A+1)\right)-\bar{\eta}\right] \quad (18)$$

where $\bar{\eta} = q/\bar{p}$ and $\bar{p} = p + \sigma_0$. For un-bonded samples ($\sigma_0 = 0$ and $A = -1$), only d_1 has an influence on the model response. It can thus be calibrated by fitting the corresponding $\varepsilon_q - \varepsilon_v$ curves in the tests.

(d) c_h and m: Under drained triaxial compression condition, one has the following relation with the small elastic deformation being neglected[1]

$$d\varepsilon_q \approx \sqrt{\frac{2}{3}}\langle dL \rangle = \sqrt{\frac{2}{3}}\frac{1-a\bar{\eta}}{K_p}dq$$
$$= \sqrt{\frac{2}{3}}\frac{(1-a\bar{\eta})(1+e)p_r}{G_0 c_h e^{[-k(A+1)+\sqrt{\sigma_0/p_r}]}(2.97-e)^2\bar{p}\sqrt{\bar{p}p_r}(M_f/\bar{\eta}-1)-(1+e)\bar{\eta}p_r m(\bar{\eta}/M_f)^{2000}\sigma_0}dq \quad (19)$$

The variable a is equal to 0 for constant-mean-stress tests and 1/3 for conventional triaxial compression tests [36]. As for un-bonded samples, c_h is the only parameter left in Eq. (19) and can be calibrated by fitting to the $\varepsilon_q - q$ curves.

The parameter m can then be determined based on the tested $\varepsilon_q - q$ relations on a cemented sand sample.

(e) c_0: Once all above parameters are determined, c_0 can be determined by fitting the $\varepsilon_q - \varepsilon_v$ curves for bonded samples under drained triaxial compression tests based on Eq. (18).

(f) k: The parameter k characterizes the stiffness anisotropy of a soil, and hence can be calibrated based on testing results of $\varepsilon_q - q$ on soils with the major principal stress direction having a deviation with the direction of deposition, according to Eq. (19). The conventional triaxial extension tests, where the major principal stress direction is perpendicular to deposition direction, is a good choice. Since k also enters the expression of D, it should be tuned based on the $\varepsilon_q - \varepsilon_v$ relations in conventional triaxial extension according to Eq. (18).

(g) v: For undrained triaxial compression tests on un-bonded sand, one has,

$$\frac{dq}{dp} = \bar{\eta} - \sqrt{\frac{3}{2}}\frac{K_p}{KD} \quad (20)$$

With all the other parameters being determined already, v can then be determined by fitting the effective stress paths in undrained triaxial compression tests. Results of $\varepsilon_q - q$ in undrained triaxial compression tests can be further used to fine tune all parameters.

---

[1] Note that the exponent to η/M_f has been adopted at a value of 2000 to make this term close to zero before the peak, but stay at 1 after the peak.
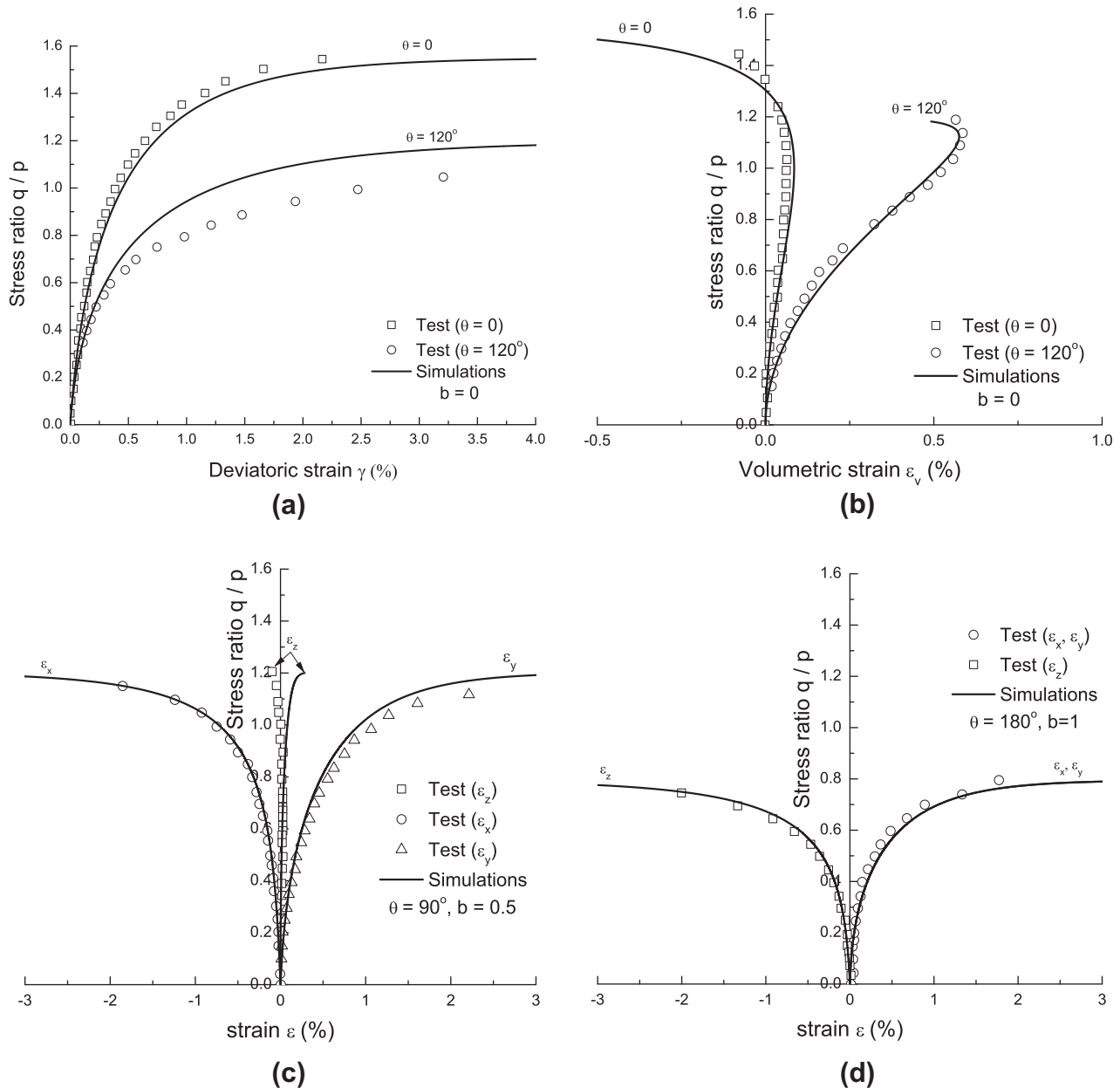
Fig. 5. Comparison between the model simulations and test results on MSP Toyoura sand in true triaxial tests. Tests and simulations have been conducted at $\theta = 0°$ and $120°$ with $b = 0$ (a and b), $\theta = 90°$ at $b = 0.5$ (c) and $\theta = 180°$ at $b = 1$ (d) (see Fig. 1a for reference).

4.2. Model verification by cemented Ottawa sand

A series of tests have been conducted by Wang and Leung [58] on cemented Ottawa sand. Since no reference has been made to the sand fabric in these tests, it is difficult for us to consider the effect of fabric anisotropy in this sand. We hereby neglect the influence of anisotropy in the following study of cemented Ottawa sand by setting the anisotropy-relevant parameters d, β and k to zero. All other related parameters have been calibrated according to the procedures outlined above. The calibrated results for the model parameters are summarized in Table 1. In particular, the initial value of bonding σ_{0i} has been calibrated with the peak strength lines of the testing data as demonstrated in Fig. 2.

Model simulations of cemented Ottawa sand samples with different cement contents under drained triaxial compression conditions and at different confining pressures are presented in Fig. 3, in comparison with the testing results as obtained by Wang and Leung [58]. As is shown in Figs. 3a and c, the predicted $\varepsilon_a - q$ relation

by our model well captures the overall trend of the deformation process observed in the tests. The increases in peak strength and stiffness with increased cement content and increased confining pressure in the tests are clearly reproduced by our model. Nevertheless, it is observed that the simulations tend to underestimate slightly the peak strength of the samples, especially for cases with the cement content at 1% and 2% and at a confining pressure of 100 kPa. This may have been caused by certain underestimations in the regression of peak strength. Meanwhile, it is found that the simulated $\varepsilon_a - e$ relations are in good agreement with the testing results for the case of confining pressure of 80 kPa. In the case of confining pressure at 100 kPa, the model predictions are reasonably good for the two cases of cement content at 0% and 3%, but slightly underestimate the volume expansion for the other two cases. In general, the effect of bonding on cemented Ottawa sand under drained shear can be captured by the proposed model with reasonable satisfaction.

As mentioned in the introduction, bonding may help to stabilize the overall structure of sand and reduce its susceptibility to lique-
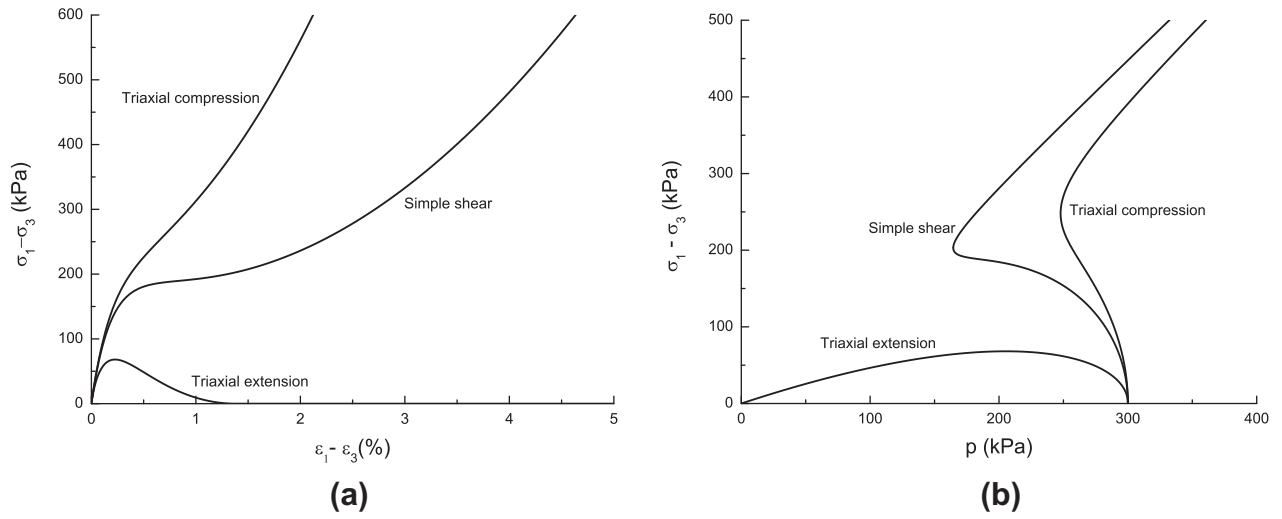
Fig. 6. Model simulations on MSP Toyoura sand under undrained loading conditions.
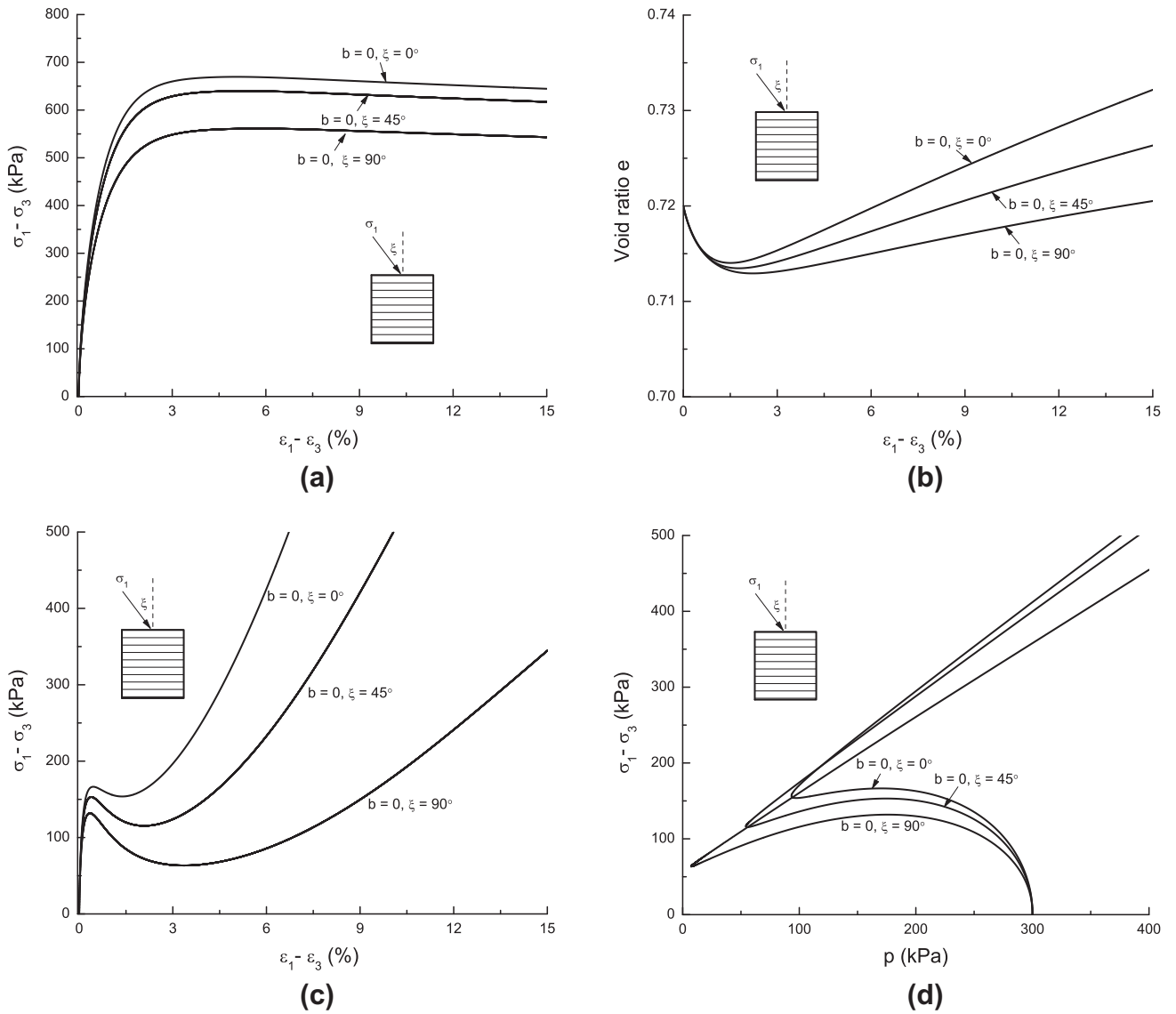

Fig. 7. Model simulations for the combined effect of bonding and fabric on sand response in drained shear (a and b) and undrained shear (c and d).

faction [9,20,32,53]. The proposed model can be employed to verify this case with undrained simulation on cemented sand. To this end, we still use cemented Ottawa sand with the model parameters listed in Table 1. In the undrained modeling, it is assumed that the samples have been compacted in the major principal stress direction before shear. The simulated results are shown in Fig. 4. As can be seen, the un-cemented sample (CC = 0%) reaches static liquefaction in the modeling, while the cemented samples are all able to pull their strength back at some phase transformation points and reach the critical state. Essentially, these cemented samples show typical response similar to medium-to-dense sand samples under triaxial compression (see e.g., [59]). As evidenced in Fig. 4c, the increase of cement content in sand may significantly reduce the maximum excess pore water pressure generated in a sample. Intuitively, the bonding created by cementation may help the soil skeleton to form a more stable structure to sustain more external shear rather than letting the pore water to share more, which may help to reduce excess pore pressure and consequently improve the resistance of sand to liquefaction. Indeed, cementation has been increasingly used as an effective means in geotechnical engineering on the stabilization of foundation soils for existing structures and for engineered slopes as well, to enhance the strength and to mitigate risks relevant to liquefaction [32].

4.3. Multiple-sieving pluviated Toyoura sand

The proposed model has also been used to predict the behavior of multiple-sieving pluviated Toyoura sand for which a number of true triaxial tests have been carried out by Miura and Toki [42]. The tests have been focused on investigating the effect of fabric on clean sand, so there is no bonding effect involved. All tests have been conducted at a constant mean stress of 196 kPa on samples with an initial relative density of D_r = 53%. The model parameters are calibrated according to the drained true triaxial testing date reported in Miura and Toki [42] and are summarized in Table 1. The deposition direction is in the direction of σ_z. Without considering the effect of bonding, we simply set the relevant parameters m and c_0 to zero. The model simulations are compared against experimental data in Fig. 5. In this figure, we use $b = (\sigma_2 - \sigma_3)/(\sigma_1 - \sigma_3)$ to denote the intermediate principal stress ratio, and its relation with θ has been shown by Ochiai and Lade [46]. The model predictions appear to compare well with the experimental data in general, only with some slight discrepancies in certain cases. The simulated $\gamma - q/p$ relation marginally overestimates the stress ratio for the case $\theta = 120°$ and $b = 0$. The maximum difference is about 11% of the measured value at around 2% deviatoric strain. The predicted ε_z for the case $\theta = 90°$ and $b = 0.5$ appears to be at odds with the measured data at high stress ratio. While it is uncertain what causes this discrepancy, it is noticed that the magnitude of tested ε_z remains very small during the entire loading course. We hence suspect the boundary constraints may have introduced some uncertainties to the experimental data on ε_z. Also notably, all tests appear to have been terminated at relatively small strain levels (e.g., around 3% of axial strain) due probably to the instrumentation restriction. Nevertheless, this may still help to justify our model simulations since constant inherent fabric anisotropy has been assumed in the model. At relative low strain level there will not be significant plastic deformation such that the fabric change that may be caused is negligible.

Likewise in the Ottawa sand case, the model simulation can be easily extended to predict the undrained response of MSP Toyoura sand. Though no testing data are available for benchmarking, the simulation may still help to understand some of the fundamental behavior of sand. Three typical loading conditions, triaxial compression, simple shear and triaxial extension are chosen for demonstration. The modeling has been performed by assuming that the initial relative density of sand samples is D_r = 53% and

the deposition plane is horizontal. The stress is applied following the procedures used by Yoshimine et al. [59]. The modeling results are shown in Fig. 6. In the figure, σ_1 and σ_3 denote the major and minor principal stress respectively; ε_1 and ε_3 denote the major and minor principal strain respectively. Stiffer and more dilative response is generally observed in the triaxial compression simulations; while more contractive and softer response is found in the triaxial extension case (static liquefaction occurs indeed in this case). The sand response under simple shear is in between the above two cases. These results are consistent with the typical phenomena observed by Yoshimine et al. [59]. On a side note, from the study it is indicative that if the evaluation of the resistance to liquefaction of sand for relevant geostructures is purely based on conventional triaxial compression tests, the strength of the soil may be overestimated, which may lead to unsafe design.

4.4. Combined effect of bonding and fabric

The current model can describe the combined effect of bonding and fabric on sand behavior. However, there are very rare relevant data in this regard. We are hence unable to perform direct comparison between the model simulations and test results. Nevertheless, a number of predictions have been made by our model on the combined effect and are shown in Fig. 7. In particular, the Ottawa sand with cement content of 3% has been used by setting d and k to be zero, as listed in the parameters for "Model illustration" in Table 1. The stress is applied following the test set-up by Yoshimine et al. [59] in hollow cylinder torsion shear apparatus, with ξ denoting the angle between the major principal stress and the direction of deposition. In all tests, the samples are initially consolidated to a confining pressure of 300 kPa. As can be seen from the drained response in Figs. 7a and b, peak strength states are observed for all three cases, which is evidently a result of bonding. At smaller ξ values, the predicted sand behavior is stiffer and more dilative under both the drained and undrained conditions (Figs. 7c and d), which reflects the effect of fabric.

5. Conclusions and discussion

An elasto-plastic constitutive model has been proposed in this paper to characterize the effect of bonding and fabric anisotropy on artificially cemented sand. The yield function employed is based on an anisotropic failure criterion for geomaterials recently proposed by the authors [22], with proper inclusion of hardening and de-bonding. The bonding is described by the triaxial tensile strength σ_0 of the material, and the fabric is characterized by a second-order fabric tensor F_{ij} originally proposed by Oda and Nakayama [47]. An anisotropic variable A, expressed by a joint invariant of the stress tensor and the fabric tensor, is employed to describe the relative orientation between the loading direction and soil fabric. All model parameters can be conveniently calibrated based on the conventional laboratory tests. Comparisons between the model simulations and test results on cemented Ottawa sand [58] as well as MSP Toyoura sand [42] are made. It is demonstrated that the model is able to capture the effect of bonding and fabric anisotropy reasonably well.

The proposed model offers a compact framework for modeling the effect of structure on sand in a comprehensive way, including both bonding and soil fabric. Admittedly, it still needs further improvements, particularly in the following respects:

(a) In the current model, the plastic deformation of sand is influenced by the fabric, and therefore, the de-bonding process is dependent on the fabric. However, it is postulated that the presence of fabric does not make the triaxial tensile strength

anisotropic. Such simplification appears to be sufficient for the cemented (grouted) sand and clean sand (no bonding). However, experimental observations on fiber-reinforced sand show that the measured cohesion is also affected by the applied loading direction [26]. In order for this model to be applicable for the fiber-reinforced sand case, proper modification of the triaxial tensile strength and its evolution with involvement of the anisotropic variable A may be an option.

(b) Notice that the bonding in the current model is assumed to be damaged due to plastic deformation. In reality, it may be weakened by elastic strain as well, similar as the damaging process of elastic degradation in micro-cracked rocks. It has also been observed that the bonding in fiber-reinforced sand may survive at large strain levels [26] (owing mainly to the fiber actually). The evolution law of de-bonding has to be carefully re-considered, e.g., by employing nonlinear relations instead of the linear ones used here, if the above situations are to be addressed.

(c) In the current model, only inherent anisotropy is considered and the soil fabric is assumed to stay unchanged during the deformation of sand. Induced anisotropy in sand can sometimes become more important in shaping the soil behavior, especially when the shear strain is high. In this case, it is mandatory to consider the evolution of soil fabric. Indeed, some preliminary attempts have been made in this regard, see, e.g., Li and Dafalias [39] and Gao et al. [21], which may likely help to open up an exciting new field for constitutive study on sand. The current model can as well be improved if the above aspects are carefully considered.

(d) The current model is proposed for artificially cemented sand with strong particles (such as silica sand or quartz sand). It may not be applicable to naturally cemented sand such as carbonate soils [12] and sandstone [5]. These latter two sands usually have high void ratio and fragile grains, and are known to exhibit high compressibility and plastic hardening predominately controlled by coupled processes of particle crushing and de-bonding. It is difficult to differentiate the two processes in laboratory conditions [5,11,12].

(e) De-bonding may be significant under isotropic compression. Indeed, as observed by Cuccovillo and Coop [12] as well as by Lo et al. [40], the behavior of weakly cemented sand with strong particles is cohesive at lower confining pressure, and becomes purely frictional when the confining pressure is very high. A plausible explanation of this would be that the bonding is damaged during the isotropic compression process before shear. While the current model is not yet able to address the de-bonding due to isotropic compression, the issue can be resolved by incorporating some existing techniques in treating the isotropic compression of structured clays into the current model, which will be pursued in a future work.

Acknowledgement

Appendix A. Details on the model derivation

Application of the condition of consistency to the general form of yield function presented in Eq. (3) results in

$$df = \frac{\partial f}{\partial \sigma_{ij}} d\sigma_{ij} + \frac{\partial f}{\partial H} dH + \frac{\partial f}{\partial \sigma_0} d\sigma_0 + \frac{\partial f}{\partial F_{ij}} dF_{ij} = 0 \quad (A.1)$$

Since the evolution of F_{ij} is not considered in this model, one has

$$df = \frac{\partial f}{\partial \sigma_{ij}} d\sigma_{ij} + \langle dL \rangle \left(\frac{\partial f}{\partial \sigma_0} \right) r_0 + \langle dL \rangle \frac{\partial f}{\partial H} r_H$$
$$= \frac{\partial f}{\partial \sigma_{ij}} d\sigma_{ij} - \langle dL \rangle K_p = 0 \quad (A.2)$$

where K_p is defined as the plastic modulus,

$$K_p = -\left[\left(\frac{\partial f}{\partial \sigma_0} \right) r_0 + \frac{\partial f}{\partial H} r_H \right] \quad (A.3)$$

Classical plasticity theory can then be followed to derive the complete constitutive relations. For the deviatoric and volumetric elastic strain increments, de_{ij}^e and $d\varepsilon_v^e$, an isotropic hypoelastic relation is postulated in the present model as follows

$$de_{ij}^e = \frac{ds_{ij}}{2G} \quad (A.4)$$

and

$$d\varepsilon_v^e = \frac{dp}{K} \quad (A.5)$$

wherein we employ expressions in Eqs. (16) and (17) for the elastic moduli K and G. For the corresponding plastic strain increments, the following relations can be obtained based on the dilatancy equation and flow rule

$$de_{ij}^p = \langle dL \rangle n_{ij} \quad (A.6)$$

and

$$d\varepsilon_v^p = D\sqrt{2/3 de_{ij}^p de_{ij}^p} = \langle dL \rangle \sqrt{2/3}D \quad (A.7)$$

where n_{ij} is defined in Eq. (15). The above equations can be used to calculate the incremental stress–strain relation. Consider the following expression

$$d\sigma_{ij} = ds_{ij} + dp\delta_{ij} = 2G de_{ij}^e + K d\varepsilon_v^e \delta_{ij}$$
$$= 2G(de_{ij} - de_{ij}^p) + K(d\varepsilon_v - d\varepsilon_v^p)\delta_{ij}$$
$$= 2G(de_{ij} - \langle dL \rangle n_{ij}) + K(d\varepsilon_v - \langle dL \rangle \sqrt{2/3}D)\delta_{ij} \quad (A.8)$$

where an additive decomposition of the total strain increment has been assumed $d\varepsilon_{ij} = d\varepsilon_{ij}^e + d\varepsilon_{ij}^p$. According to Eqs. (A.2)–(A.8), the expression for the loading index can be obtained as,

$$\langle dL \rangle = \frac{2G \frac{\partial f}{\partial \sigma_{ij}} + \left(K - \frac{2G}{3} \right) \frac{\partial f}{\partial \sigma_{kl}} \delta_{kl} \delta_{ij}}{\frac{\partial f}{\partial \sigma_{ij}} \left(2G n_{ij} + \sqrt{\frac{2}{3}} K D \delta_{ij} \right) + K_p} d\varepsilon_{ij} = \Theta_{ij} d\varepsilon_{ij} \quad (A.9)$$

Combining Eqs. (A.8) and (A.9), one can get the following incremental form constitutive relation which is ready for numerical computations,

$$d\sigma_{ij} = \Lambda_{ijkl} d\varepsilon_{kl} \quad (A.10)$$

where

$$\Lambda_{ijkl} = G(\delta_{ik}\delta_{jl} + \delta_{il}\delta_{jk}) + (K - 2G/3)\delta_{ij}\delta_{kl} - h(dL)(2G n_{ij} + \sqrt{2/3}K D \delta_{ij})\Theta_{kl} \quad (A.11)$$

where $h(dL)$ is the Heaviside step function, with $h(dL > 0) = 1$ and $h(dL \leqslant 0) = 0$.

Appendix B. Partial derivatives

For the reader's convenience of further reference, we also derive and provide the results for all the partial derivatives used in the proposed model. According to the chain rule, one can get the following

$$\frac{\partial f}{\partial \sigma_{ij}} = \frac{\partial f}{\partial \bar{\sigma}_{kl}} \frac{\partial \bar{\sigma}_{kl}}{\partial \sigma_{ij}} + \frac{\partial f}{\partial A} \frac{\partial A}{\partial \sigma_{ij}}$$

$$= \left(\frac{\partial f}{\partial \bar{I}_1} \frac{\partial \bar{I}_1}{\partial \bar{\sigma}_{kl}} + \frac{\partial f}{\partial \bar{I}_2} \frac{\partial \bar{I}_2}{\partial \bar{\sigma}_{kl}} + \frac{\partial f}{\partial \bar{I}_3} \frac{\partial \bar{I}_3}{\partial \bar{\sigma}_{kl}} \right) \frac{\partial \bar{\sigma}_{kl}}{\partial \sigma_{ij}} + \frac{\partial f}{\partial A} \frac{\partial A}{\partial \sigma_{ij}} \tag{B.1}$$

where

$$\frac{\partial f}{\partial \bar{I}_1} = \frac{\alpha \bar{I}_1}{\sqrt{\bar{I}_1^2 - 3\bar{I}_2}} + \frac{2(1-\alpha)\sqrt{x-9}}{3\sqrt{x-1} - \sqrt{x-9}} + y\frac{\bar{I}_2}{\bar{I}_3} - \frac{1}{3}Hg(A) \tag{B.2}$$

$$\frac{\partial f}{\partial \bar{I}_2} = \frac{-3\alpha}{2\sqrt{\bar{I}_1^2 - 3\bar{I}_2}} + y\frac{\bar{I}_1}{\bar{I}_3} \tag{B.3}$$

$$\frac{\partial f}{\partial \bar{I}_3} = -y\frac{\bar{I}_1\bar{I}_2}{\bar{I}_3^2} \tag{B.4}$$

in which

$$x = \frac{\bar{I}_1\bar{I}_2}{\bar{I}_3}, \quad y = \frac{24(1-\alpha)\bar{I}_1}{(3\sqrt{x-1} - \sqrt{x-9})^2\sqrt{(x-1)(x-9)}} \tag{B.5}$$

and

$$\frac{\partial \bar{I}_1}{\partial \bar{\sigma}_{ij}} = \delta_{ij}, \quad \frac{\partial \bar{I}_2}{\partial \bar{\sigma}_{ij}} = \bar{I}_1\delta_{ij} - \bar{\sigma}_{ij}, \quad \frac{\partial \bar{I}_3}{\partial \bar{\sigma}_{ij}} = \bar{\sigma}_{ik}\bar{\sigma}_{kj} + \bar{I}_2\delta_{ij} - \bar{I}_1\bar{\sigma}_{ij} \tag{B.6}$$

$$\frac{\partial \bar{\sigma}_{mn}}{\partial \sigma_{ij}} = \delta_{mi}\delta_{nj} \tag{B.7}$$

$$\frac{\partial f}{\partial A} = -\frac{1}{3}\bar{I}_1Hg(A)[2d(A+1) + d\beta] \tag{B.8}$$

$$\frac{\partial A}{\partial \sigma_{ij}} = \frac{d_{ij}}{\sqrt{d_{kl}d_{kl}}\sqrt{s_{pq}s_{pq}}} - \frac{3}{2}\frac{A}{q^2}s_{ij} \tag{B.9}$$

By combining Eqs. (B.1)–(B.9), $\frac{\partial f}{\partial \sigma_{ij}}$ can be calculated. Finally, the following two expressions are also needed in formulating the constitutive relations

$$\frac{\partial f}{\partial \sigma_0} = \frac{\partial f}{\partial \bar{\sigma}_{ij}}\delta_{ij}, \quad \frac{\partial f}{\partial H} = -\frac{1}{3}\bar{I}_1g(A) \tag{B.10}$$

References

[1] Abdulla AA, Kiousis PD. Behavior of cemented sands-II. Modelling. Int J Numer Anal Methods Geomech 1997;21:549–68.
[2] Asghari E, Toll DG, Haeri SM. Triaxial behaviour of a cemented gravely sand, Tehran alluvium. Geotech Geol Eng 2003;21:1–28.
[3] Baudet B, Stallebrass S. A constitutive model for structured clays. Géotechnique 2004;54:269–78.
[4] Belokas G, Kavvadas M. An anisotropic model for structured soils part I: theory. Comput Geotech 2010;37:737–47.
[5] Bica AVD, Bressani LA, Vendramin DM, Martins FB, Ferreira PMV, Gobbi F. Anisotropic shear strength of a residual soil of sandstone. Can Geotech J 2008;45:367–76.
[6] Burland JB. On the compressibility and shear strength of natural clays. Géotechnique 1990;40:329–78.
[7] Casagrande A, Carillo N. Shear failure of anisotropic materials. Proc Boston Soc Civil Eng 1944;31:74–87.
[8] Chazallon C, Hicher PY. A constitutive model coupling elastoplasticity and damage for cohesive-frictional materials. Mech Cohes Frict Mater 1998;3:41–63.
[9] Clough GW, Iwabuchi J, Rad NS, Kuppusamy T. Influence of cementation on liquefaction of sands. J Geotech Eng 1989;115:1102–17.
[10] Consoli NC, Foppa D, Festugato L, Heineck KS. Key parameters for strength control of artificially cemented soils. J Geotech Eng 2007;133:197–205.
[11] Coop MR, Atkinson JH. The mechanics of cemented carbonate sands. Géotechnique 1993;43:53–67.
[12] Cuccovillo T, Coop MR. On the mechanics of structured sands. Géotechnique 1999;49:741–60.
[13] Dafalias YF, Papadimitriou AG, Li XS. Sand plasticity model accounting for inherent fabric anisotropy. J Eng Mech 2004;130:1319–33.
[14] Dano C, Hicher PY. Behavior of uncemented sands and grouted sands before peak strength. Soils Found 2003;43:13–9.
[15] Desai CS, Toth J. Disturbed state constitutive modeling based on stress–strain and nondestructive behaviors. Int J Solids Struct 1996;33:1619–50.
[16] Díaz-Rodríguez JA, Antonio-Izarraras VM, Bandini P, López-Molina JA. Cyclic strength of a natural liquefiable sand stabilized with colloidal silica grout. Can Geotech J 2008;45:1345–55.
[17] Fernandez AL, Santamarina JC. Effect of cementation on the small-strain parameters of sands. Can Geotech J 2001;38:91–199.
[18] Gajo A, Muir Wood D. A new approach to anisotropic, bounding surface plasticity: general formulation and simulations of natural and reconstituted clay behaviour. Int J Numer Anal Methods Geomech 2001;25:207–41.
[19] Galavi V, Schweiger HF. A multilaminate model with destructuration considering anisotropic strength and anisotropic bonding. Soils Found 2009;49:341–53.
[20] Gallagher PM, Mitchell JK. Influence of colloidal silica grout on liquefaction potential and cyclic undrained behavior of loose sand. J Soil Dynam Earthquake Eng 2002;22:1017–26.
[21] Gao ZW, Zhao JD, Li XS, Dafalias YF. Fabric evolution and dilatancy in modeling the anisotropic behavior of granular materials; in preparation.
[22] Gao ZW, Zhao JD, Yao YP. A generalized anisotropic failure criterion for geomaterials. Int J Solids Struct 2010;47:3166–85.
[23] Hicher PY, Chang CS, Dano C. Multi-scale modeling of grouted sand behavior. Int J Solids Struct 2008;45:4362–74.
[24] Hirai H, Takahashi M, Yamada M. An elastic–plastic constitutive model for the behavior of improved sandy soils. Soils Found 1989;29:69–84.
[25] Huang JT, Airey DW. Properties of artificially cemented carbonate sand. J Geotech Geoenviron Eng 1998;124:492–9.
[26] Ibraim E, Diambra A, Muir Wood D, Russell AR. Static liquefaction of fibre reinforced sand under monotonic loading. Geotext Geomembr 2010;28:374–85.
[27] Ismael NF. Properties and behavior of cemented sand deposits in Kuwait. Soils Found 1999;39:47–57.
[28] Kachanov LM. On the creep rupture time. Izv Akad Nauk SSSR Otd Tekh Nauk 1958;8:26–31.
[29] Kaga M, Yonekura R. Estimation of strength of silicate-grouted sand. Soils Found 1991;31:43–59.
[30] Kasama K, Zen K, Iwataki K. Undrained shear strength of cement-treated soils. Soils Found 2006;46(2):221–32.
[31] Kavvadas M, Amorosi A. A constitutive model for structured soils. Géotechnique 2000;50:263–73.
[32] Kodaka T, Ohno Y, Takyu T. Cyclic shear characteristics of treated sand with colloidal silica grout. In: Proceedings of the 16th international conference on soil mechanics and geotechnical engineering, Osaka; 2005. p. 401–4.
[33] Lade PV. Three-parameter failure criterion for concrete. J Eng Mech Div 1982;108(5):850–63.
[34] Lagioia R, Nova R. An experimental and theoretical study of the behaviour of a calcarenite in triaxial compression. Géotechnique 1995;45:633–48.
[35] Leroueil S, Vaughan PR. The general and congruent effects of structure in natural soils and weak rocks. Géotechnique 1990;40(3):67–488.
[36] Li XS, Dafalias YF. Dilatancy for cohesionless soils. Géotechnique 2000;50(4):449–60.
[37] Li XS, Dafalias YF. Constitutive modeling of inherently anisotropic sand behavior. J Geotech Geoenviron Eng 2002;128:868–80.
[38] Li XS, Dafalias YF. A constitutive framework for anisotropic sand including non-proportional loading. Géotechnique 2004;54:41–55.
[39] Li XS, Dafalias YF. Anisotropic critical state theory: the role of fabric. J Eng Mech; 2011. doi:10.1061/(ASCE)EM.1943-7889.0000324.
[40] Lo SCR, Lade PV, Wardani SPR. An experimental study of the mechanics of two weakly cemented soils. Geotech Testing J 2003;26(3):1–14.
[41] Mitrani H, Madabhushi SPG. Cementation liquefaction remediation for existing buildings. Ground Improvement 2010;163:81–94.
[42] Miura S, Toki S. Elastoplastic stress–strain relationship for loose sands with anisotropic fabric under three-dimensional stress conditions. Soils Found 1984;24(2):43–57.
[43] Namikawa T, Mihira S. Elasto-plastic model for cement-treated sand. Int J Numer Anal Methods Geomech 2007;31:71–107.
[44] Nishimura S, Minh NA, Jardine RJ. Shear strength anisotropy of natural London Clay. Géotechnique 2007;57:49–62.
[45] Nova R, Castellanza R, Tamagnini C. A constitutive model for bonded geomaterials subject to mechanical and/or chemical degradation. Int J Numer Anal Methods Geomech 2003;27:705–32.
[46] Ochiai H, Lade PV. Three-dimensional behavior of sand with anisotropic fabric. J Geotech Eng 1983;109:1313–28.
[47] Oda M, Nakayama H. Yield function for soil with anisotropic fabric. J Eng Mech 1989;115:89–104.
[48] Pietruszczak S. On inelastic behaviour of anisotropic frictional materials. Mech Cohes Frict Mater 1999;4:281–93.
[49] Reddy KR, Saxena SK. Effects of cementation on stress–strain and strength characteristics of sands. Soils Found 1993;33:121–34.
[50] Richart FE, Hall JR, Woods RD. Vibrations of soils and foundations. Englewood Cliffs, New Jersey: Prentice-Hall Inc.; 1970.
[51] Rotta GV, Consoli NC, Prietto PDM, Coop MR, Graham J. Isotropic yielding in an artificially cemented soil cured under stress. Géotechnique 2003;53:493–501.
[52] Saebimoghaddam A. Liquefaction of early age cemented paste backfill. PhD thesis, University of Toronto, Toronto; 2009.

[53] Saxena SK, Reddy KR, Avramidis AS. Liquefaction resistance of artificially cemented sand. J Geotech Eng 1988;114:1395–413.

[54] Sekiguchi H, Ohta K. Induced anisotropy and time dependency in clays. In: Constitutive equations of soils proceedings of the 9th international conference on soil mechanics and foundation engineering special session 9, Tokyo; 1977. p. 229–38.

[55] Sun DA, Matsuoka H. An elastoplastic model for frictional and cohesive materials and its application to cemented sands. Mech Cohes Frict Mater 1999;4:525–43.

[56] Vatsala A, Nova R, Srinivasa Murthy BR. Elastoplastic model for cemented soils. J Geotech Geoenviron Eng 2001;127:679–87.

[57] Wan RG, Guo PJ. Effect of microstructure on undrained behaviour of sands. Can Geotech J 2001;38:16–8.

[58] Wang YH, Leung SC. Characterization of cemented sand by experimental and numerical investigations. J Geotech Geoenviron Eng 2008; 134:992–1004.

[59] Yoshimine M, Ishihara K, Vargas W. Effects of principal stress direction and intermediate principal stress on undrained shear behavior of sand. Soils Found 1998;38:179–88.

[60] Yu YZ, Pu JL, Ugai K. A damage model for soil–cement mixture. Soils Found 1998;38:1–12.

[61] Zhao JD, Sheng DC, Rouainia M, Sloan SW. Explicit stress integration of complex soil models. Int J Numer Anal Methods Geomech 2005; 29:1209–29.